J. exp. Biol. 148, 53–88 (1990)
Printed in Great Britain © *The Company of Biologists Limited 1990*

MECHANICS OF FORWARD FLIGHT IN BUMBLEBEES

II. QUASI-STEADY LIFT AND POWER REQUIREMENTS

BY R. DUDLEY* AND C. P. ELLINGTON

Department of Zoology, University of Cambridge, Downing Street, Cambridge CB2 3EJ, United Kingdom

Accepted 2 June 1989

Summary

This paper examines the aerodynamics and power requirements of forward flight in bumblebees. Measurements were made of the steady-state lift and drag forces acting on bumblebee wings and bodies. The aerodynamic force and pitching moment balances for bumblebees previously filmed in free flight were calculated. A detailed aerodynamic analysis was used to show that quasi-steady aerodynamic mechanisms are inadequate to explain even fast forward flight. Calculations of the mechanical power requirements of forward flight show that the power required to fly is independent of airspeed over a range from hovering flight to an airspeed of $4{\cdot}5\,m\,s^{-1}$.

Introduction

A biomechanical analysis of forward flight in insects requires initially a description of the kinematics of flight, and then proceeds to an understanding of the aerodynamics and mechanics associated with these kinematics. Wing and body kinematics of bumblebees in forward flight were given previously (Dudley & Ellington, 1990); this paper analyzes the ensuing aerodynamic forces and mechanical power requirements. Results of steady-state lift and drag measurements on bumblebee wings and bodies are first presented. A quasi-steady aerodynamic analysis is then used to evaluate the likelihood of unsteady aerodynamic mechanisms operating during forward flight. Finally, estimates are made of the mechanical power requirements of flight at different airspeeds.

For an aerodynamic analysis of forward flight in insects, it is necessary to evaluate the overall balance of forces. A vertical force must be produced to support the body weight. Similarly, a horizontal thrust is required to balance the drag force acting on the body of the insect. This so-called parasite drag, the aerodynamic force acting parallel to the airflow on the fuselage of a flying machine, is, in general, proportional to the square of the forward airspeed and can be a significant component of the overall force balance. Lift forces on the body, which act perpendicularly to the drag, may also be of significance for flying insects,

* Present address: Smithsonian Tropical Research Institute, APO Miami, FL 34002, USA.

Key words: aerodynamics, power, flight, bumblebees.

by reducing the net lift required from the beating wings (Hocking, 1953). If accurate calculations of power requirements are to be made, it is essential to have detailed information about the lift and drag forces acting on insect bodies. Similarly, for an aerodynamic analysis of forward flight, knowledge is required of the aerodynamic characteristics of wings at the appropriate Reynolds numbers. No such data are available for bumblebee wings, although the wings of various other insects have been studied (e.g. Jensen, 1956; Vogel, 1967; Nachtigall, 1977, 1981). An aerodynamic evaluation of insect wings may also reveal particularly advantageous adaptations or modifications of the insect wing (e.g. Rees, 1975*a*,*b*; Newman *et al.* 1977). To provide the data necessary for a mechanical analysis of forward flight, a systematic study of the aerodynamic characteristics of bumblebee wings and bodies was undertaken.

A fundamental question in insect flight aerodynamics is whether steady-state aerodynamics are sufficient to provide the horizontal and vertical forces necessary for flight. One method of evaluating the possible importance of unsteady aerodynamics is to compare mean lift and mean profile drag coefficients, as calculated from kinematic data and the overall force balance, with experimental measurements of steady-state lift and drag on real wings (Osborne, 1951; Weis-Fogh, 1973). Ellington (1984*a*) provides a review of the quasi-steady aerodynamic analysis of animal flight. The flapping wing is conceptually reduced to a series of aerodynamic sections operating at specific angles of attack and instantaneous velocities; any effects of wake vorticity, acceleration and deceleration of the wing, and wing rotation are ignored. Forces on each section are determined according to conventional aerodynamic theory. In the mean coefficient method of Osborne (1951), mean values of the lift and drag coefficients of the wing, as averaged along the wing and through the wingbeat, are determined from the horizontal and vertical force balance. The mean lift coefficient $\overline{C}_L$ represents the minimum value of the lift coefficient that is compatible with steady-state aerodynamics; if lift coefficients vary during the wingbeat, then some instantaneous values must exceed $\overline{C}_L$. Unsteady aerodynamic effects are therefore implicated if $\overline{C}_L$ is greater than the maximum lift coefficient measured at the appropriate Reynolds numbers on real wings. There exist relatively few investigations of the mean force coefficients required for forward flight in animals and, with one exception (Osborne, 1951), these studies are confined to vertebrate flight (Pennycuick, 1968*b*; Norberg, 1976).

The mean coefficient method is used here to determine force coefficients for bumblebees previously filmed in forward flight and for which detailed kinematic and morphological data are available (Dudley & Ellington, 1990). A modified version of the force balance method of Norberg (1976) is used to find the mean lift and drag coefficients necessary to provide the requisite lift and thrust for flight at each forward airspeed, while lift coefficients for hovering flight are determined according to the equations derived by Ellington (1984*d*).

Given accurate knowledge of the kinematics of flapping flight, calculations of the associated energetic costs are possible. In the past, attention has been given to the variation of mechanical power requirements with forward airspeed, the so-

called power curve. The total mechanical power required for flight can be determined by summing the individual components of parasite power, induced power, profile power and inertial power. Aerodynamic theories that predict the form and characteristics of the power curve have been proposed and applied to the kinematics of flying birds and bats (e.g. Pennycuick, 1968*b*, 1975; Tucker, 1973; Greenewalt, 1975; Rayner, 1979). Variation of mechanical power requirements with forward airspeed has not been previously examined for free-flying insects.

Mechanical power requirements and metabolic power input are related by the overall efficiency of the flight muscle. If muscle efficiency does not vary with airspeed, the form of the curve relating metabolic power input to airspeed will be the same as that for mechanical power output. Power curves relating metabolic rates to airspeed have been determined for free-flying birds (e.g. Tucker, 1966, 1972; Bernstein *et al.* 1973; Torre-Bueno & LaRochelle, 1978; Berger, 1985) and for free-flying bats (e.g. Thomas, 1975, 1981; Carpenter, 1985). Some of these curves are similar to those predicted by theory, although they are in general much shallower than expected and yield minimum power airspeeds different from theoretical values. For comparative purposes, therefore, it is of particular interest to determine power curves for insects in flight over a range of airspeeds.

Calculations of the mechanical power output of bumblebees previously filmed in free flight were made by summing at each flight speed the individual components of parasite, induced, profile and inertial power. By comparing, for each insect, the maximum power output of the thoracic muscle with the calculated power output incorporating inertial power requirements, it was possible to evaluate the likelihood of elastic energy storage during the wingbeat (when the latter quantity exceeds the former, some elastic energy storage is necessary). Power curves for forward flight were determined by calculating mechanical power requirements at three different forward airspeeds and for hovering flight.

Materials and methods

A list of abbreviations is given in the Appendix of Dudley & Ellington (1990).

Steady-state lift and drag measurements

Force measurements were made with the optoelectronic force transducer shown in Fig. 1. The test object was attached to an entomological pin 27 mm in length and 0·3 mm in diameter. A length of 3·5 mm stainless-steel tubing was attached to a spring element at the top of the transducer, and at the bottom it was connected to the mounting needle. The angle of attack of the test object was changed by rotating the mounting needle at this point. The spring elements were made from stainless-steel tubing of varying diameters according to the desired mechanical response of the system. Application of a force to the test object resulted in very small displacements of the central tubing, which were measured with two infrared LED–photodiode pairs (Texas Instruments TIL31A, TIL81). An arbitrary displacement of the tubing was resolved into two orthogonal components. Movement of the central tubing during experiments was very small, of the order of

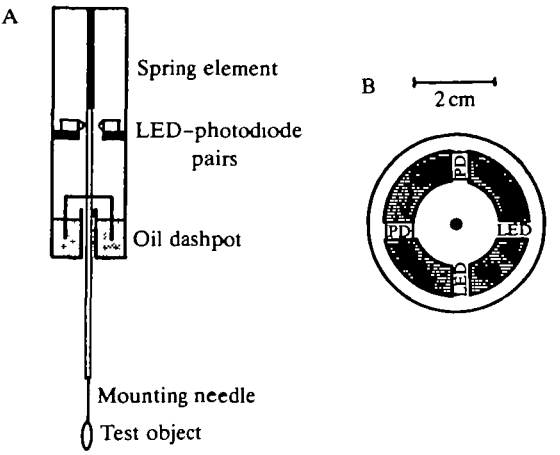

Fig. 1. (A) Side-view of the force transducer used in all measurements. (B) Cross-sectional view of the transducer at the level of the LED–photodiode (PD) pairs.

1 μm at the point of measurement. The optical center of each LED–photodiode pair was offset from the vertical axis of the transducer by a distance equal to the radius of the central tubing (Fig. 1B). Metal windows were positioned in front of the photodiodes to block off part of the infrared beam and thereby allow higher amplification of the photodiode signal. An oil dashpot was mounted below the level of the photodiodes, and vertical adjustment of a cylindrical drag vane mounted on the central tubing permitted adjustment of the damping force until critical damping was achieved. The transducer was constructed of an aluminum alloy (Dural), and all interior surfaces were painted black to minimize stray reflectance from the LEDs.

The output of each photodiode was put through a two-stage amplifier with facilities for d.c. offset and variable gain. Signal output ranged from -13 to $+13$ V, typical peak-to-peak noise averaged less than 30 mV, and signal drift with time was less than $10\,\mathrm{mV\,h^{-1}}$. The signal was either displayed on a chart recorder or converted into a digital signal by means of a twelve-bit A–D converter (CUBAN-12, Control Universal Ltd) connected to a Model B BBC microcomputer.

The transducer was mounted rigidly on a heavy Palmer stand, which rested upon a foam-rubber pad to reduce extraneous vibration. The entire system was levelled by means of a three-point support at the base of the stand. The transducer was positioned above the exit of the open-jet tunnel (see below) such that the mounting needle projected through the sharply defined interface between still air and the jet of the tunnel. The test object was located in the uniform flow of the tunnel typically 2 cm below this interface. Drag forces on the mounting needle were therefore minimized and, in general, were less than 5 % of the drag force acting on the test object. Any possible aerodynamic interaction between the test object and the mounting needle was presumed to be minimal.

The orientation of the transducer relative to the wind tunnel was such that the

optical axis of one LED–photodiode pair was parallel to the oncoming flow of air, thereby responding to drag forces acting on the test object; the other LED–photodiode pair responded to forces acting orthogonal to the drag, i.e. to the lift force. This orientation was checked by verifying that no lift forces registered by the transducer were generated by flat plates positioned parallel to the air flow.

The wind tunnel used in all aerodynamic force measurements was the same as that used by Weis-Fogh (1956), except that the original motor was replaced with a d.c. motor for better speed control. Tunnel velocity was monitored with a bead thermistor anemometer (Prosser AVM 502). Average velocity fluctuations in the region of force measurement were small, typically 3 % of the mean velocity.

The transducer was calibrated independently for lift and drag by applying known forces horizontally to the mounting needle in the necessary orthogonal directions. Because displacement of the steel tubing at the level of the LEDs was dependent upon the point of application of force along the length of the mounting needle, the transducer was calibrated with forces applied at three points with an 8 mm spacing along the mounting needle. At any particular point, the relationship between applied force and transducer output was almost exactly linear. For a particular test object, and therefore a particular point of force application, force coefficients were determined by interpolation or extrapolation from the calibration curves. For mounted insect bodies, aerodynamic force was presumed to act at the point of intersection of the mounting needle and the medial plane of the insect (see below). The aerodynamic force on insect wings was assumed to act through the radius of the second moment of wing area (Weis-Fogh, 1973).

Specimens of the bumblebee *Bombus terrestris* (L.) (Hymenoptera: Apidae) *sensu* Alford (1975) were collected in the Cambridge University Botanic Garden. The bumblebee was identified using Alford (1975). Force measurements on wings and bodies were always made on the day of insect capture. Insects were killed for use in experiments by exposure to chloroform vapor.

For force measurements on bodies, only those insect bodies which displayed a posture similar to that in free flight were used. Wings of the insect were removed by cutting through the wing base articulation. Because of the difficulties involved in mounting insect legs in an orientation resembling that in free flight, all legs were cut from the body at the base of the coxae. Concomitant changes in volume and cross-sectional area of the insect fuselage are small, and should not significantly affect force measurements. The insect body was then rigidly mounted by inserting the tip of the mounting needle through one wing base and forcing the needle through the thoracic musculature until the tip emerged through the opposite wing base. A measurement with Vernier calipers of the wing base separation was made at this stage to determine the point of aerodynamic force application upon the mounting needle.

Measurements of parasite drag and body lift were made over a wide range of body angles relative to the oncoming wind. When the longitudinal axis of the insect body was parallel to the axis of the wind tunnel, the body angle was defined as 0°; positive body angles indicate a 'nose-up' attitude, i.e. increased exposure of

the ventral surface of the insect body to the oncoming airflow. Lift and drag were determined at 15° intervals, starting at −15° and increasing to 60°. Measurements were made at five different wind velocities (1, 2, 3, 4 and 5 $m\,s^{-1}$) to investigate the dependence of aerodynamic characteristics upon the Reynolds number. The Reynolds number (*Re*) is given by Ul/ν, where U is the air speed, ν the kinematic viscosity of air ($1{\cdot}46\times10^{-5}\,m^2\,s^{-1}$), and l is either the body length, in the case of insect bodies, or the mean chord, in the case of insect wings. Photographs were taken of the mounted insect bodies at 0° and 90°, and were used to determine the maximum projected area at these orientations.

Wings used in force measurements were cut from the insect body just proximal to the articulation and perpendicular to the wing span. A small drop of melted beeswax was placed on the base of the cut wing, and the tip of the mounting needle was then inserted into the hardening wax. For bumblebee wings, fore- and hindwing bases were stuck together with a small amount of wax, and the mounting needle was then attached in the region of the forewing base. This mounting of the fore- and hindwing was carried out very carefully to ensure that the two wings were realistically coupled together.

Force measurements on wings were made over the same velocity range used for insect bodies. Angles of attack typically ranged from −40° to +50°, the interval between measurements being 10°. For some wings, measurements between 0° and 30° were made at 5° intervals. Angle of attack here refers to the geometrical angle of the wing chord relative to the longitudinal axis of the tunnel. The 0° angle of attack for bumblebee wings proved to be difficult to define, as the wing is twisted by 15°–25° along the wing span. The wing chord used to define the angle of attack was taken at approximately one-third the wing length, as the extent of twisting is less in proximal regions of the wing. For some bumblebee wings, the angle between the fore- and hindwing was altered from the standard orientation by bending the two wings at a point between the two waxed wing bases; the resulting line of flexion corresponded approximately to the longitudinal flexion line of the forewing. The angle between the two wings was determined from a 35 mm photograph.

Full-scale models of bumblebee wings were made from 0·02 mm flat copper sheet. The angle between the fore- and hindwing of the bumblebee model, which was an outline of the overlapped wings, could be changed easily. Mild camber could also be imparted to the model wings. Force measurements for these copper models were made at the same wind velocities and angles of attack as for real insect wings.

Lift and drag coefficients (C_L and C_D, respectively) were determined from force measurements according to the following formulae:

$$L = \tfrac{1}{2}\rho C_L A U^2 , \tag{1}$$

$$D = \tfrac{1}{2}\rho C_D A U^2 , \tag{2}$$

where ρ is the density of air ($1{\cdot}23\,kg\,m^{-3}$), A is a reference area, U is the wind

velocity, D is the drag force, and L is the lift. For insect wings, planform area (the horizontally projected area at 0° angle of attack) was used as the reference area to calculate force coefficients. For insect bodies, a planform area equal to the product of the body length and the mean body diameter (see Dudley & Ellington, 1990) was used as the reference area.

Passive pitching moments

For the three bumblebees filmed for kinematic analysis (Dudley & Ellington, 1989), passive pitching moments generated by the airflow about the bodies were determined. The insect bodies were pinned through the wing bases, with the pin mounted on horizontal supports such that there was free rotation of the body about the wing base axis. The mounted body was placed in the jet of the wind tunnel, which was operated at speeds of 1, 2·5 and 4·5 m s^{-1}. At each airspeed, a 35 mm photograph of the insect was taken to determine the body angle relative to horizontal.

The passive pitching moment M_p generated about the wingbase axis by the moving air is given by:

$$M_p = mgl_1\sin(\chi' - \chi_0) , \quad (3)$$

where m is the mass of the insect, g is gravitational acceleration, l_1 is the distance from the wingbase axis to the center of mass, χ_0 is the free body angle, and χ' is the body angle resulting from passive pitching moments at a particular airspeed (Fig. 2). The magnitude and direction of the resultant force F acting on the body were estimated from force coefficient data at the appropriate body angle χ' and Re (see Results). The distance from the wing base axis l through which the resultant force acts on the body was determined by equating the moment of the resultant force perpendicular to the longitudinal body axis with the actual moment required to maintain the observed body angle. Values of l were found to be relatively independent of χ' and Re. For each insect, therefore, a mean value was determined for the ratio of l to l_1, the radius of the first moment of body mass about the wing base axis. Values of l/l_1 are as follows: BB01, 4·54; BB02, 4·46; BB03, 1·03. Coefficients of variation for these mean values averaged 19 %. Given

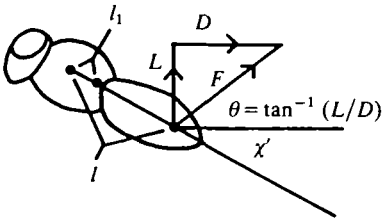

Fig. 2. Body angle χ' resulting from passive pitching moments, with the aerodynamic force F acting at a distance l from the wing base axis. θ, angle of elevation; D, lift force; L, drag force; l_1, distance from wing base axis to center of mass.

l, it is then possible to determine, at any body angle χ and resultant force F, the passive pitching moment generated by airflow past the body:

$$M_p = lF\sin(\theta+\chi) , \quad (4)$$

where

$$\theta = \tan^{-1}(L/D) .$$

Passive pitching moments for bumblebees in free flight were determined from equation 4.

The quasi-steady aerodynamic analysis

The following equations, taken directly or modified from Norberg (1976), permit a calculation of the vertical and horizontal components of the wing lift and drag (equations 8–11). The body weight minus the body lift is balanced by the vertical components, and the body drag by the horizontal components. It is then possible to solve for the mean lift and drag coefficients as averaged along the wing and through the wingbeat (equations 12 and 13).

Relative velocity

To determine the forces acting on a wing section, it is necessary to know the relative velocity acting on the wing. This quantity is determined from the vector sum of the flapping velocity, the induced velocity and the forward airspeed.

The flapping velocity $v(r,t)$ of a wing section at distance r from the wing base and at time t is given by:

$$v(r,t) = r\pi\Phi n\sin(2\pi nt) , \quad (5)$$

where Φ is the stroke amplitude and n is the wingbeat frequency. It is assumed in calculations of the flapping velocity that the wing motion follows simple harmonic motion and is confined to the stroke plane. These are justifiable approximations, given the observed wingbeat kinematics of bumblebees in free forward flight (Dudley & Ellington, 1989).

The induced velocity V_i is assumed to be constant across the wing and through the wingbeat. Using the Rankine–Froude momentum theory of propellors, the induced velocity can be calculated from:

$$V_i = mg/2\rho A_0(V^2 + V_i^2)^{1/2} , \quad (6)$$

where ρ is the density of air, V is the forward airspeed and A_0 is the area of the actuator disc, the latter being the surface over which a pressure impulse is applied to the air (Bramwell, 1976). Although previous authors have generally taken as the actuator disc a circular disc with radius equal to the wing length (e.g. Weis-Fogh, 1973; Rayner, 1979), we here follow Ellington (1984*c*) in using for the actuator disc the area $\Phi R^2\cos\beta$, where Φ is given in radians. This definition of the disc area corresponds to the horizontal projection of the wing stroke which, because V_i is assumed to be always directed downwards, ensures that the disc area corresponds to only that area through which downward momentum is imparted to the air. A disc area of πR^2 will seriously underestimate the induced velocity in

hovering and slow flight (e.g. Ellington, 1984*c*) and, for the advance ratios typical of bumblebee flight, use of the horizontal projection of the actual area swept out by the wings is most appropriate.

The relative velocity $V_R(r,t)$ was then determined from the vector sum of the flapping velocity, the induced velocity and the forward airspeed. In the quasi-steady analysis, span-wise components of flow are presumed not to contribute to aerodynamic force production; the relative velocity was therefore calculated as that component of the vector sum normal to the longitudinal axis of the wing. The equations presented by Norberg (1976) fail to determine the component of the induced velocity normal to the wing span, and take as this quantity simply the magnitude of the induced velocity. The normal component of the induced velocity, $V_{i,norm}$, was used in the present calculations of the relative velocity. It is determined from V_i by:

$$V_{i,norm} = V_i \cos\sigma , \tag{7}$$

where

$$\sigma = \tan^{-1}\left(\frac{\sin\phi\sin\beta}{\cos\phi}\right)$$

Force components

The vertical components of the lift and drag forces are given by equations 8 and 9, respectively:

$$L_{vert}(r,t) = \tfrac{1}{2}\rho V_R^2(r,t)A(r)C_L(r,t)\cos\Psi(1-\cos^2\phi\sin^2\beta)^{1/2} , \tag{8}$$

$$D_{vert}(r,t) = \tfrac{1}{2}\rho V_R^2(r,t)A(r)C_D(r,t)\sin\Psi(1-\cos^2\phi\sin^2\beta)^{1/2} , \tag{9}$$

and the horizontal components by equations 10 and 11, respectively:

$$L_{hor}(r,t) = \tfrac{1}{2}\rho V_R^2(r,t)A(r)C_L(r,t)\sin\Psi\cos\epsilon , \tag{10}$$

$$D_{hor}(r,t) = \tfrac{1}{2}\rho V_R^2(r,t)A(r)C_D(r,t)\cos\Psi\cos\epsilon , \tag{11}$$

Here, $A(r)$ is the area of a wing section at distance r from the wing base, V_R is the resultant velocity, and $C_L(r,t)$ and $C_D(r,t)$ are the instantaneous lift and drag coefficients. The angle Ψ is the angle between the relative velocity and horizontal, and the angle ϵ is the arctan of the ratio of the components of the induced velocity and forward airspeed in planes normal to the longitudinal wing axis (Norberg, 1976).

To determine the direction of forces produced on the wing, it is necessary to know the sign of the effective angle of incidence of the wing as well as the direction of the relative velocity vector (given by Ψ); the direction of the lift force on the wing is reversed when effective angles of incidence are negative. Geometrical angles of attack, α, of wing sections through the wingbeat were taken from Dudley & Ellington (1990), intermediate data points being determined by linear interpolation. The effective angle of attack of a wing section was determined from the direction of the relative velocity and the geometrical angle of attack. The effective angle of incidence is then given by the effective angle of attack minus the zero-lift angle of attack of the wing. As will be seen in the Results, it is difficult to specify

exactly the zero-lift angle of bumblebee wings: it is negative, as would be expected from cambered wings, and for the purposes of these calculations is arbitrarily taken to be $-10°$. Calculations using zero-lift angles ranging from $0°$ to $-15°$ did not significantly affect the results.

Mean force coefficients

The sum of vertical components of lift and drag on the two wings, when integrated along the wing and over the wingbeat period, equals the weight *mg* (less any lift on the body L_b) integrated over the same time. Similarly, the horizontal components of the lift and drag on the wings must equal the horizontal drag on the body. By assuming that the force coefficients are constant (i.e. that the wing is operating at a constant effective angle of incidence), it is possible to solve for the mean lift coefficient $\overline{C}_L$ and mean drag coefficient $\overline{C}_D$ from equations 12 and 13:

$$mg - L_b = \overline{C}_L \rho n \int_0^T \int_0^R V_R^2(r,t)c(r)\cos\Psi(1-\cos^2\phi\sin^2\beta)^{1/2}\mathrm{d}r\mathrm{d}t + \overline{C}_D \rho n \int_0^T \int_0^R V_R^2(r,t)c(r)\sin\Psi(1-\cos^2\phi\sin^2\beta)^{1/2}\mathrm{d}r\mathrm{d}t\,, \quad (12)$$

$$D_b = \overline{C}_L \rho n \int_0^T \int_0^R V_R^2(r,t)c(r)\sin\Psi\cos\epsilon\mathrm{d}r\mathrm{d}t + \overline{C}_D \rho n \int_0^T \int_0^R V_R^2(r,t)c(r)\cos\Psi\cos\epsilon\mathrm{d}r\mathrm{d}t\,, \quad (13)$$

where n is the wingbeat frequency, T is the wingbeat period, c is the wing chord, and D_b is the parasite drag on the body.

A BASIC program encoding the mean coefficients method was written for a BBC Model B microcomputer. All kinematic and morphological data necessary for the calculations were taken from Dudley & Ellington (1990). The wing was conceptually divided into the three span-wise sections for which mean geometrical angles of attack had previously been determined; the area of each wing had previously been measured in the analysis of wing morphology. Mean values of the lift and drag coefficients, averaged along the wing and through the wingbeat, were determined from equations 12 and 13. Mean lift coefficients of the wings during hovering flight were calculated according to the equations of Ellington (1984*d*).

If the wingbeat kinematics determined from short high-speed film sequences deviate substantially from the mean values measured over a longer period, then substantial variation may be introduced into calculations of mean lift coefficients. For the three bumblebees filmed previously in free flight, no systematic variation with airspeed was observed for the stroke amplitude, mean positional angle or wingbeat frequency. Mean values for kinematic parameters were therefore calculated for each individual using the values obtained at each of the forward airspeeds and for hovering. Lift coefficients were calculated with these mean kinematic values as well as with the actual values determined at each airspeed, in order to determine the sensitivity of the results to short-term kinematic variation.

Mechanical power output

Mechanical power output of insects filmed in free flight was determined by summing the parasite, induced, profile and inertial powers. Rather than determining aerodynamic power requirements through a consideration of the aerodynamic torque on the wings (e.g. Weis-Fogh, 1973; Norberg, 1976), we calculated the components separately, because it is doubtful whether the induced drag component of the total drag coefficient for wings in steady airflow is appropriate for the induced drag of flapping wings. Power is simply drag multiplied by speed, so parasite power P_{par} is given by the product of body drag and forward airspeed. The induced power P_{ind} is given by the product of the induced velocity V_i and the weight of the insect. The instantaneous profile power P_{pro} of the flapping wings is equal to the product of the profile drag and the resultant velocity, V_R, and is calculated from:

$$P_{pro} = \rho C_{D,pro} \int_0^R c(r) V_R{}^3 dr \,, \tag{14}$$

where $C_{D,pro}$ is the profile drag coefficient of the wing. The mean profile power averaged over the wingbeat was determined.

The choice of an appropriate profile drag coefficient was a somewhat arbitrary one. Given the effective angles of incidence at which the wings are operating (see Results), $C_{D,pro}$ is unlikely to exceed 0·3. For the *Re* of the wings based on the mean velocity and mean chord (1000–2000), the equation for profile drag coefficients given by Ellington (1984*d*) predicts values around 0·2. Profile power requirements were therefore calculated with profile drag coefficients of 0·1 and 0·3 to cover the range of likely values.

The power P_{acc} required to accelerate the mass and virtual mass of the wing pair during the first half of a half-stroke is given by:

$$P_{acc} = 2nI(d\phi/dt)_{max}{}^2 \,, \tag{15}$$

where I is the moment of inertia of the wing and the wing virtual mass (Ellington, 1984*d*), and $(d\phi/dt)_{max}$ is the maximum angular velocity. It was assumed that the wing follows simple harmonic motion and is confined to the stroke plane; the maximum angular velocity was calculated accordingly. Using the morphological parameters given in Dudley & Ellington (1990), I is calculated from:

$$I = \rho_w S R^3 \hat{h} \hat{r}_2{}^2(m) + \tfrac{1}{8}\pi\rho S^2 R \hat{v} \hat{r}_2{}^2(v) \,, \tag{16}$$

where ρ_w is the wing mass density, $\hat{h}$ is the mean wing thickness divided by wing length, $\hat{r}_2(m)$ is the non-dimensional radius of the second moment of wing mass, $\hat{v}$ is the virtual mass of the wing pair, $\hat{r}_2(v)$ is the non-dimensional radius of the second moment of wing virtual mass, and S is wing area.

Total power requirements were calculated for the two cases of perfect elastic energy storage (P_{acc} supplied by elastic strain energy) and zero elastic energy storage. In the latter case, muscles must perform negative work to decelerate the wings at the end of each half-stroke. For vertebrate striated muscle, the metabolic

energy required to perform negative work is much less than that required for an equivalent amount of positive work (Margaria, 1968), and in previous studies of animal flight the cost of negative work has been assumed to be negligible (e.g. Norberg, 1976; Ellington, 1984*d*). In the present study, negative work was also neglected, and inertial power requirements averaged over a half-stroke are then equal to half the value of P_{acc}, as given by equation 15.

In addition to the mechanical power requirements described above, there exist at least two additional avenues of energy expenditure. First, the basal metabolism must be added to the power requirements of flight. Unlike birds and bats, however, basal metabolic rates of insects are only 1–2 % of the metabolic rates in flight (Kammer & Heinrich, 1978), and this contribution to the power curve is usually ignored. Second, the cost of physiological support systems, such as increased energy demands of circulation and respiration, must also be included. These are difficult to evaluate and are generally assumed to be negligible for flying insects.

Total mechanical power output was divided by the body mass to yield body mass-specific mechanical power requirements. Calculations of mechanical power requirements in hovering flight were made using the equations derived by Ellington (1984*d*); the profile power requirements in hovering flight, as for forward flight, were calculated using profile drag coefficients of 0·1 and 0·3.

Results

Body drag and lift

Within each of two groups examined (bumblebee queens and bumblebee workers), the insects were of sufficiently similar size that no systematic variation of lift and drag coefficients with body mass was found. Mean values of force coefficients for five individuals were therefore determined. Because variation in body length was relatively small within a group, a mean *Re* based on the mean body length was also determined. For each group, Table 1 presents mean body mass, mean body length, mean plan area, and mean frontal area at a body angle of 0°; force coefficients calculated with the planform area based on body length and mean body diameter can therefore easily be transformed to those based on frontal area or other reference areas. The variation of mean body drag coefficients with

Table 1. *Mean morphological data for bumblebees used in the calculation of mean force coefficients*

	m (mg)	l_b (mm)	S_{plan} (mm^2)	$S_{frontal}$ (mm^2)
Bumblebee queens	555·2 (48)	20·4 (0·79)	168 (16·1)	86·6 (24·3)
Bumblebee workers	197·6 (30)	18·6 (0·43)	102 (10·0)	56·5 (12·7)

Each value represents the mean of five individuals, with one standard error given in parentheses.

Variables as follows: m, body mass; l_b, body length; S_{plan}, plan area based on mean body diameter; $S_{frontal}$, frontal area at a body angle of 0°.

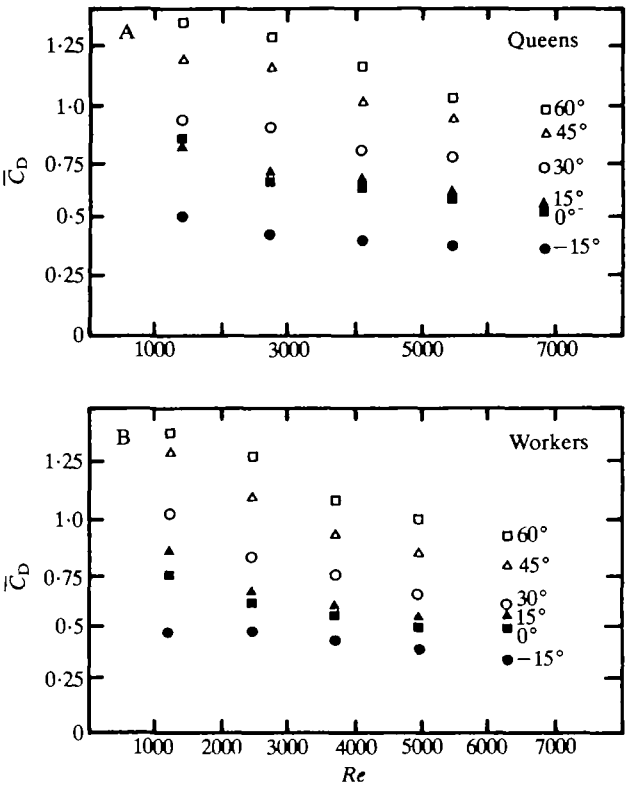

Fig. 3. Mean body drag coefficients $\overline{C}_D$ based on plan area *versus* mean Reynolds number (*Re*) for (A) five bumblebee queens and (B) five bumblebee workers, at six different body angles. Standard errors were independent of body angle and *Re*; the mean standard error was 0·02 for bumblebee queens and 0·035 for bumblebee workers.

the mean *Re* and with body angle is given in Fig. 3A (bumblebee queens) and Fig. 3B (bumblebee workers). Results for mean lift coefficients are presented in Fig. 4. Lift and drag forces were not, in general, proportional to the square of the airspeed but to some smaller power. Force coefficients therefore tended to decrease with increased *Re*. Lift forces were typically 20–50 % of the drag forces, even at large body angles. The magnitude of the drag force was, however, always relatively small in comparison to the weight of the insect. Body force coefficients were all consistent with quasi-steady aerodynamics (see Discussion).

Aerodynamic forces and pitching moments

Morphological and kinematic data were used in conjunction with force coefficient data to calculate the lift and drag forces on the bodies of those bumblebees previously filmed in free forward flight (Dudley & Ellington, 1990). The body weight (minus the body lift) and the body drag must be balanced by the mean aerodynamic lift and thrust produced by the beating wings. Any influence of the induced velocity field on the body is ignored. Body drag and lift coefficients

were taken from Figs 3 and 4, respectively; values for intermediate body angles and flight speeds were determined by linear interpolation. For the same film sequences analyzed for wing kinematics, body drag and lift as a function of forward airspeed are given in Fig. 5. As has been previously reported for other large insects (e.g. Weis-Fogh, 1956; Nachtigall, 1964), the ratio of body drag to body weight is relatively small even at high airspeeds.

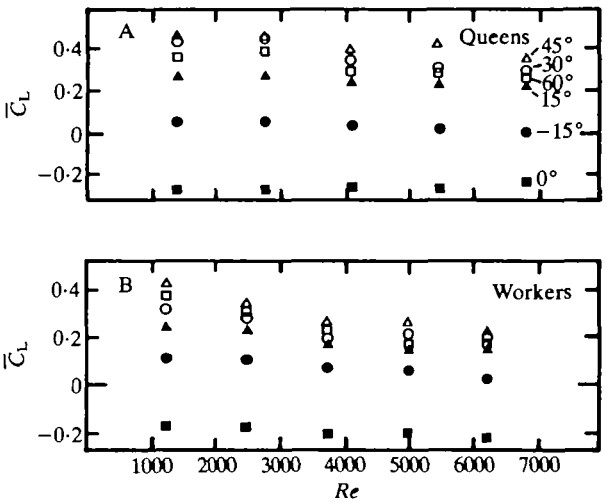

Fig. 4. Mean body lift coefficients $\overline{C}_L$ based on plan area *versus* mean Reynolds number (*Re*) for (A) five bumblebee queens and (B) five bumblebee workers, at six different body angles. Standard errors were independent of body angle and *Re*; the mean standard error was 0·025 for bumblebee queens and 0·021 for bumblebee workers.

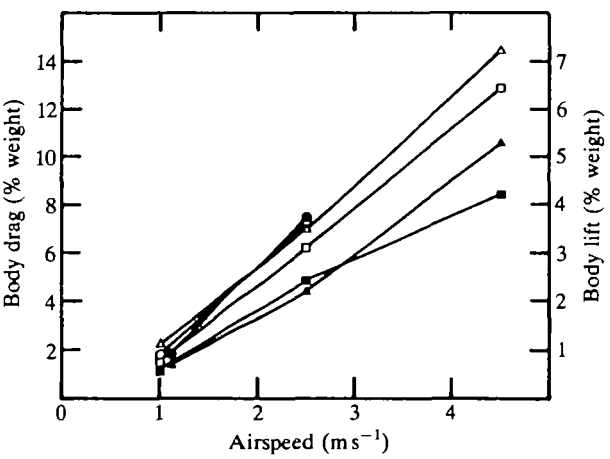

Fig. 5. The variation with airspeed of the body drag (open symbols) and lift (closed symbols), expressed as a percentage of body weight. Symbols refer to the insects described in Dudley & Ellington (1990): squares, BB01; triangles, BB02; circles, BB03.

The net vertical force F_{vert} required from the wings is equal to the weight of the insect minus the vertical body lift. The net horizontal force F_{hor} required is simply equal to the horizontal body drag. The magnitude F of the resultant force vector is given by $(F_{vert}^2+F_{hor}^2)^{1/2}$, and its angular tilt γ from the vertical by the arctangent of F_{hor}/F_{vert}. Values of γ are typically 1°, 4° and 8° at airspeeds of 1, 2·5 and 4·5 m s^{-1}, respectively. At any particular airspeed, therefore, the rotation of the resultant force vector is much smaller than that of the stroke plane of the wings (see Dudley & Ellington, 1990).

The variations with forward airspeed of the passive pitching moment M_p and the pitching moment M (the moment required to tilt the body to the body angle χ observed in free flight) are given in Fig. 6. The moment M is determined from:

$$M = mgl_1\sin(\chi-\chi_0)\ . \tag{17}$$

Values of M are typically greater than those of M_p. Assuming in a quasi-steady analysis that the net aerodynamic force acts through the second radius of wing area (Weis-Fogh, 1973), the predicted moment M_{qs} generated by the wings may be derived as:

$$M_{qs} = F_{vert}R\hat{r}_2(S)\sin\bar{\phi}\cos\beta\ . \tag{18}$$

Using kinematic data previously given, the pitching moment M_{qs} predicted by equation 18 may be compared with the actual pitching moment M required to produce the observed body angle; the ratio of these two quantities is given in Fig. 7. The moment predicted by a quasi-steady analysis is typically twice the necessary value.

Wing characteristics

Force measurements were made on the wing of one bumblebee queen and one

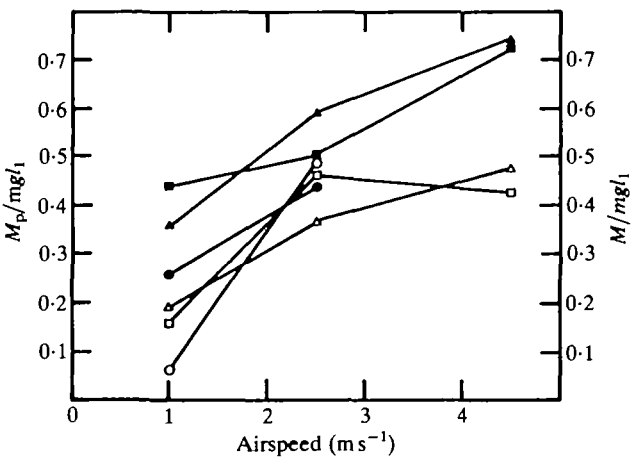

Fig. 6. Variation of the passive pitching moment M_p (open symbols) and the required pitching moment M (closed symbols) with airspeed. Both moments are made non-dimensional by dividing by mgl_1. Symbols as follows: squares, BB01; triangles, BB02; circles, BB03.

bumblebee worker. Fig. 8 gives polar diagrams for positive angles of attack at three different airspeeds for the bumblebee worker wing. Lift increases with increasing angle of attack until a maximum lift coefficient, $C_{L,max}$, is reached, and then gradually decreases. Maximum lift coefficients generally occurred at angles of attack between 25° and 30°. Lift coefficients of bumblebee wings were lower in absolute magnitude at negative angles of attack than when arranged at positive

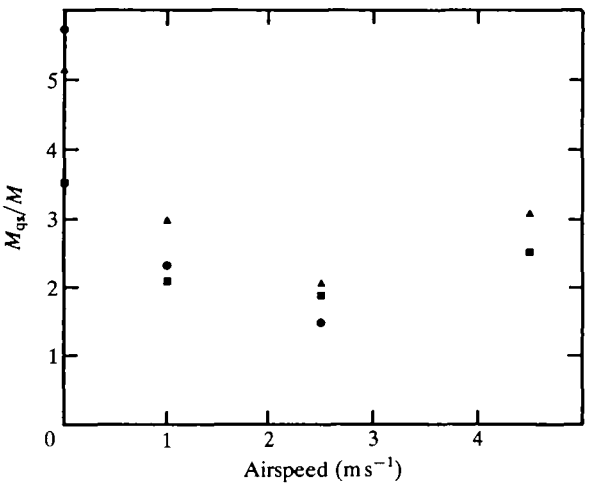

Fig. 7. Variation with airspeed of the ratio of the pitching moment predicted by a quasi-steady analysis, M_{qs}, to the moment, M, required to maintain the observed body angle in free flight. Symbols as in Fig. 6.

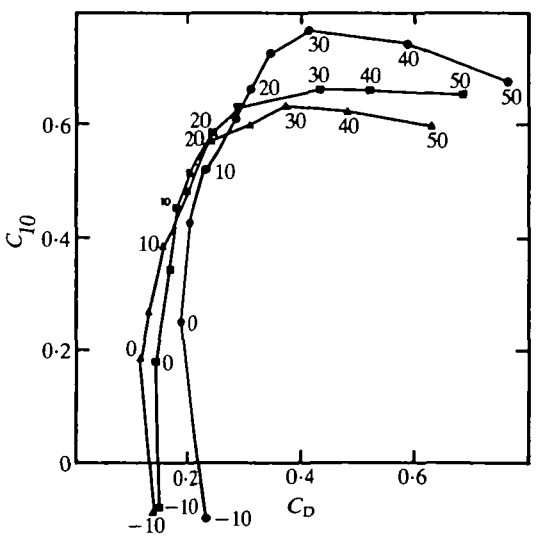

Fig. 8. Polar diagrams for a bumblebee wing, 11·2 mm in length. Airspeeds of 2 (●), 3 (■), and 5 (▲) $m s^{-1}$ correspond to *Re* based on the mean wing chord of 470, 700 and 1170, respectively. Angles of attack in degrees are indicated parametrically on the curve.

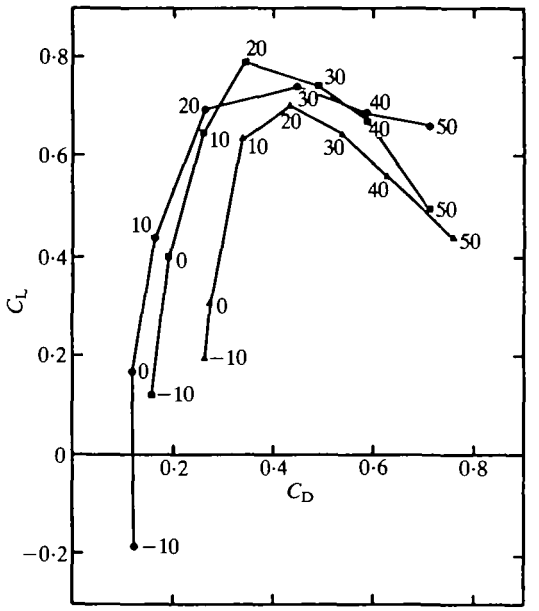

Fig. 9. Polar diagrams for a bumblebee queen wing (length 15·4 mm) with the hindwing in the normal position (●), and set at 35° (■) and 54° (▲). Airspeed is 5 m s^{-1}, *Re* is 1530. Angles of attack in degrees are indicated parametrically on the curves.

angles. Both the minimum drag coefficient, $C_{D,min}$, and the maximum lift coefficient, $C_{L,max}$, tended to decrease with increased *Re* (see Table 2).

Fig. 9 shows the effects of a variable hindwing angle on the polar diagram of a queen bumblebee wing. An increased hindwing angle of 35° increased the lift coefficient of the wing by as much as 50 % at angles of incidence less than 20°. A concomitant increase in the drag coefficient at any particular angle of attack of the wing was also observed. Maximum lift coefficients generally declined at greater hindwing angles; for a hindwing angle of 54°, the wing polar diagram shifts downwards and even further to the right. In the forward flight of bumblebees, hindwing deflection of the magnitude considered here is characteristic (Dudley & Ellington, 1990).

Table 2 presents, for two airspeeds, certain parameters of aerodynamic performance for a bumblebee worker wing and a bumblebee queen wing with the hindwing arranged at different angles.

Steady-state aerodynamics

Effective angles of incidence

Advance ratios for bumblebees in forward flight were always less than 1 (Dudley & Ellington, 1990) and even at an airspeed of 4·5 m s^{-1} were typically 0·6–0·7, indicating that the mean flapping velocity was always greater than the flight velocity. Thus, in a quasi-steady analysis, forces will be largely governed by the

Table 2. *Aerodynamic characteristics of bumblebee wings at two airspeeds*

	1	2	3	4
Airspeed of $2\,m\,s^{-1}$				
$C_{L,max}$	0·77	0·79	0·90	0·81
$C_{D,min}$	0·25	0·18	0·21	0·34
L/D_{max}	2·26	2·57	2·66	1·75
$C_{L,max}/C_{L,50°}$	1·13	1·04	1·64	1·50
$C_{D,f}$	0·124	0·108	0·110	0·112
Re	460	610	580	560
Airspeed of $5\,m\,s^{-1}$				
$C_{L,max}$	0·64	0·75	0·80	0·71
$C_{D,min}$	0·13	0·12	0·18	0·28
L/D_{max}	2·48	2·75	2·50	1·89
$C_{L,max}/C_{L,50°}$	1·07	1·13	1·64	1·60
$C_{D,f}$	0·076	0·068	0·070	0·071
Re	1240	1520	1450	1390

Identification as follows: (1) wing (fore- and hindwing) of bumblebee worker, wing length 12·2 mm; (2) wing of bumblebee queen, length 15·4 mm; (3) same wing of bumblebee queen with hindwing angle of 35°; (4) same wing of bumblebee queen with hindwing angle of 54°.

The Reynolds number *Re* is based on the mean wing chord.

The friction drag coefficient $C_{D,f}$ is determined from equation 19 in the text. C_L, lift coefficient; L, lift; D, drag.

flapping velocity during the half-stroke rather than by the forward velocity predominant at the ends of half-strokes. Mean values for the effective angles of incidence for the upstroke were therefore calculated ignoring the periods of wing rotation at the ends of half-strokes. Inclusion of the periods of wing rotation in calculations of mean effective angles of incidence necessarily increases their variance, but does not alter the general conclusions presented below.

Mean effective angles of incidence were always positive, which means that air strikes the ventral surface of the wing on the downstroke and the dorsal surface on the upstroke. Mean effective angles of incidence for the upstroke and downstroke typically ranged from 20° to 40°, with 95 % confidence intervals typically ±5° to ±10°. In only four of the 23 sequences of forward flight examined did the mean effective angle of incidence during the upstroke differ significantly from that during the downstroke, but never by more than 20°. The difference in mean effective angles of incidence between the downstroke and upstroke was in all other cases less than 10°. No consistent relationship was found between the mean effective angle of incidence during a half-stroke and forward airspeed. Additionally, there was no significant span-wise variation in effective angles of incidence. The high mean effective angles of incidence suggest that in forward flight, as in hovering flight, the wing is operating near the plateau of the polar diagram. The polar diagrams in Figs 8 and 9 include the effects of the induced velocity, and effective angles of incidence of the wings will actually be somewhat less than the

angles of attack quoted. Given the high and relatively constant mean effective angles of incidence, and the absence of a difference between the downstroke and upstroke means, the assumption of a constant lift coefficient (probably near the maximum lift coefficient) throughout the wingbeat is justified.

Force balance and force coefficients

Because body drag is very small in comparison to body weight, and also in comparison to the horizontal components of the wing force, small errors in the calculated direction of these forces can lead to significant problems with the horizontal force balance. Indeed, solving equations 12 and 13 simultaneously often resulted in the physical impossibility of negative drag coefficients. Errors in the magnitude and direction of the forces on the wing can easily arise from inaccuracies in the estimate of the induced velocity, which is assumed to be constant along the wing and through the wingbeat. This estimate also ignores effects of vorticity in the wake, as well as interference at the ends of half-strokes arising from bound vorticity on the opposite wing. Even small errors in the calculated relative velocity and effective angles of incidence resulting from these effects will disturb the delicate horizontal force balance. It was therefore decided to consider only the vertical force balance, and to investigate, for a range of realistic values of the mean drag coefficient, the resulting mean lift coefficients and mechanical power requirements. Assuming a mean drag coefficient different from that calculated according to equations 12 and 13 means that the horizontal force balance is not satisfied, but for the drag coefficients used this results in a negligible change in the magnitude (1 %) and direction (5°) of the resultant force produced by the beating wings.

Drag coefficients measured on real insect wings reflect a contribution of the induced drag, and actual profile drag coefficients will be somewhat lower than those given above. Considering the polar diagrams for bumblebee wings, and the calculated mean effective angles of incidence, it is unlikely that mean profile drag coefficients will exceed 0·3. Also, the mean profile drag coefficient cannot be less than the minimum profile drag coefficient for a flat plate parallel to flow. For the Reynolds numbers appropriate to forward flight, this value will be near 0·1. Since profile drag coefficients measured on real wings reflect some additional component of pressure drag, the minimum profile drag coefficient of real wings will be somewhat higher. Ellington (1984*d*) used minimum profile drag coefficients between 0·1 and 0·3 to estimate profile power requirements in hovering flight. In the present study, calculations of the mean lift coefficient were made using equation 12, with mean drag coefficients of 0·1 and 0·3 as likely extremes of the continuum of possible drag coefficients. The mean drag coefficient of 0·3 corresponds approximately to operation of the wing near the middle of the plateau of the polar diagram.

Fig. 10 shows the variation with airspeed of mean lift coefficients for the three bumblebee sequences analyzed in Dudley & Ellington (1990). Mean lift coefficients were always greater than one, and never varied by more than 10 % when

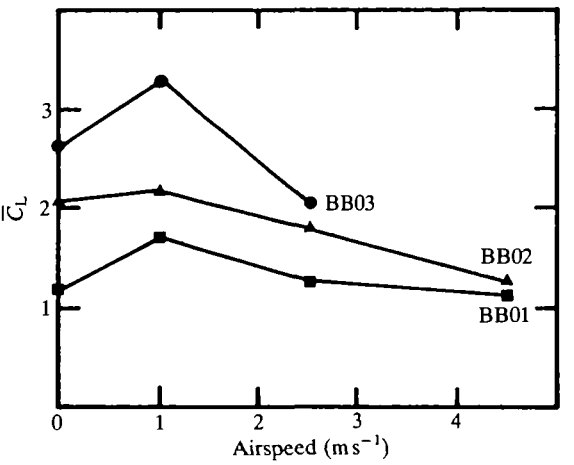

Fig. 10. Variation with airspeed of the mean lift coefficient $\overline{C}_L$, calculated according to quasi-steady aerodynamic theory. The mean profile drag coefficient is equal to 0·1.

the mean drag coefficient increased from 0·1 to 0·3. Excluding the case of hovering flight, mean lift coefficients showed a general tendency to increase with decreased airspeed. No significant differences resulted when actual wing kinematic parameters at particular airspeeds were used instead of mean values.

Relative contributions of the downstroke and upstroke

The vertical forces produced during the wingbeat were calculated from equations 8–11 by substituting the mean lift coefficient and the assumed mean drag coefficient for the instantaneous lift and drag coefficients. Fig. 11 shows the contribution of the downstroke to the total vertical forces produced during the wingbeat. Weight support in hovering flight is assumed to be equal for the two

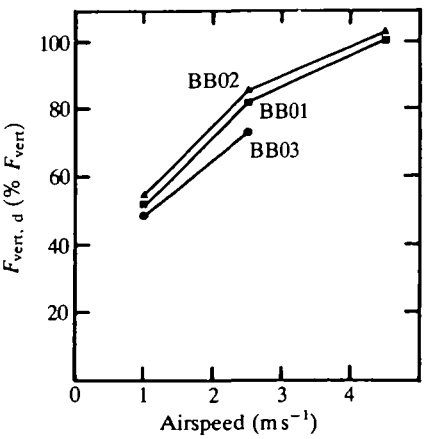

Fig. 11. Vertical force produced by the wings during the downstroke, $F_{vert,d}$, as a percentage of the total vertical force, F_{vert}, produced during the wingbeat.

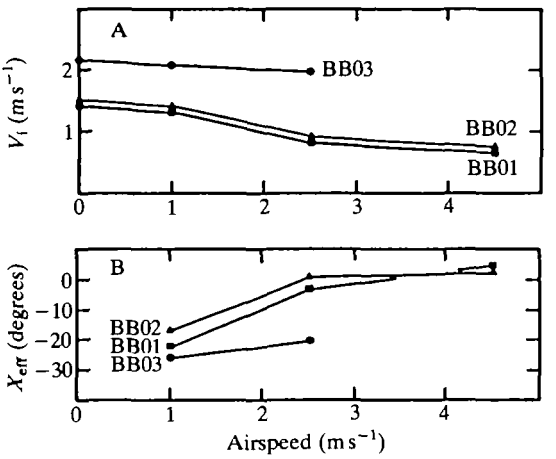

Fig. 12. (A) Induced velocity V_i as a function of airspeed. (B) Effective body angle χ_{eff} as a function of airspeed.

half-strokes (see Ellington, 1984*d*). It can be seen that as airspeed increases the contribution of the downstroke to vertical force production increases; that of the upstroke correspondingly decreases.

Induced velocity

Fig. 12A shows the variation with forward airspeed of the induced velocity, V_i, calculated according to equation 6. The induced velocity is typically greater than 1 m s^{-1}, and is thus comparable to the forward airspeed. Fig. 12B gives as a function of airspeed the effective body angle, χ_{eff}, the body angle relative to the resultant of the forward airspeed and the induced velocity. It can be seen that in most cases effective body angles are negative, indicating that the induced velocity as calculated above will substantially alter flow in the region of the body. Inclusion of the induced velocity vector in calculations of body drag has, however, little effect. At airspeeds of 2·5 and 4·5 m s^{-1}, the induced velocity reduces body drag by about 10 %. Only at an airspeed of 1 m s^{-1} does body drag increase, by up to 30 %. At higher airspeeds, body drag is reduced because of a decrease in effective body angle and an increase in *Re*, both trends tending to reduce the body drag coefficient.

Mechanical power output

The variation of the individual power components with airspeed was similar for all insects, and is illustrated for the insect BB01 in Fig. 13A (using mean kinematic parameters) and Fig. 13B (which uses the actual kinematic parameters measured at particular airspeeds). The contribution of parasite power to the power curve was usually very small. Induced power requirements decreased and profile power requirements increased substantially with increased airspeed, the sum of the two components remaining approximately constant. Inertial power requirements

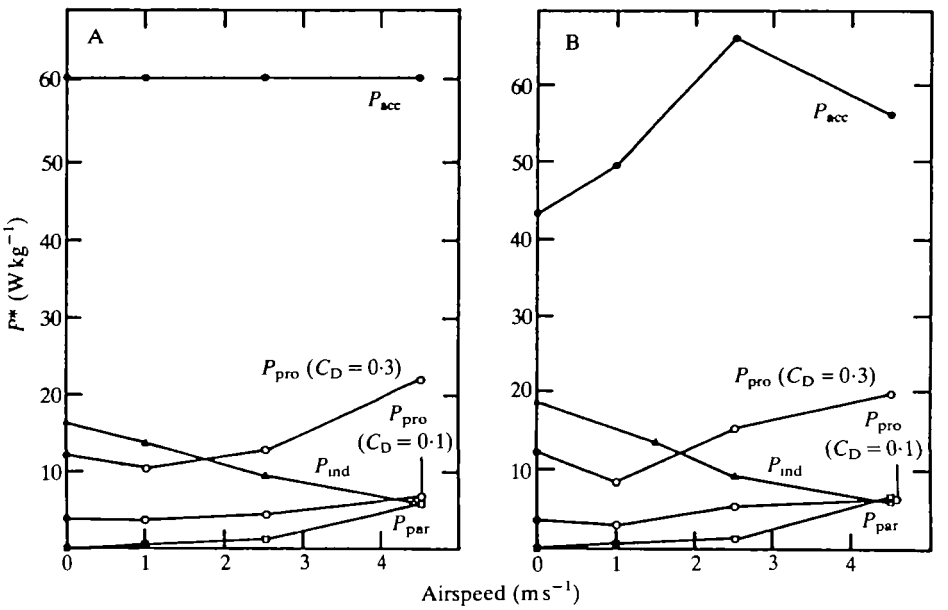

Fig. 13. Individual components of the power curve for the insect BB01, calculated with (A) mean kinematics and (B) actual kinematic values for each airspeed. P_{par}, parasite power; P_{ind}, induced power; P_{pro}, profile power; P_{acc}, power required to accelerate wing mass and virtual mass over the first half of a half-stroke.

averaged over a half-stroke were, in general, greater than the sum of the other components averaged over the same time interval. Curves calculated with mean kinematic values were generally much smoother than those determined with actual kinematic values at each airspeed. The power curves to follow were all calculated using mean kinematic parameters.

For all bumblebees, the variation of body mass-specific mechanical power output, P^*, with forward airspeed is given in Fig. 14 for perfect elastic energy storage and in Fig. 15 for zero elastic energy storage. In general, the mechanical power curves exhibit very shallow minima, and mechanical power requirements are approximately independent of forward airspeed.

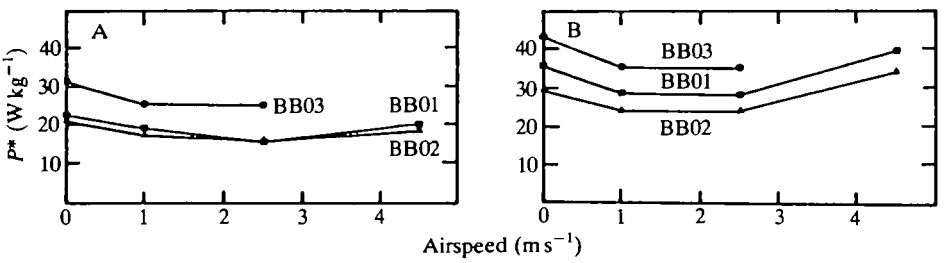

Fig. 14. Variation of body mass-specific mechanical power output, P^*, with airspeed, assuming perfect elastic energy storage. (A) Mean profile drag coefficient of 0·1. (B) Mean profile drag coefficient of 0·3.

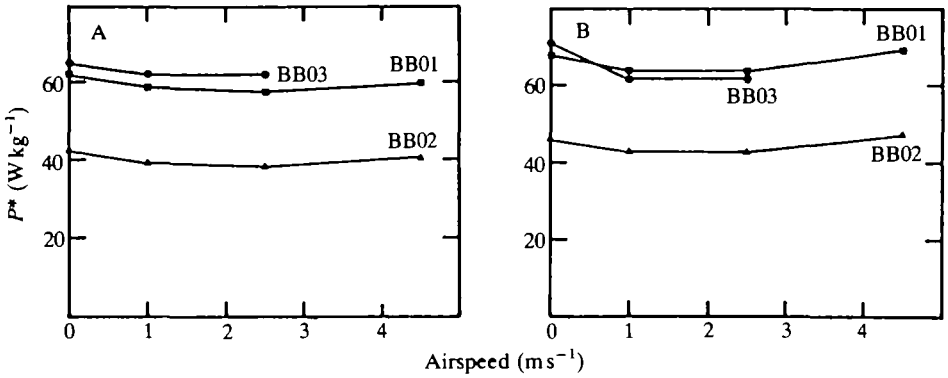

Fig. 15. Variation of body-mass specific mechanical power output P^* with airspeed, assuming zero elastic energy storage. (A) Mean profile drag coefficient of 0·1. (B) Mean profile drag coefficient of 0·3.

An aerodynamic efficiency η_a may be determined from the ratio of the induced power to the sum of the profile and induced powers. Values of η_a ranged from 0·3 to 0·6, and tended to decrease with increased airspeed. Values calculated for hovering flight were comparable to those determined by Ellington (1984*d*).

Discussion

Body drag

In general, detailed drag coefficient data are not available for the *Re* range relevant to insect flight. The body drag coefficients (based on plan area) obtained in the present study ranged from 0·12 to 0·95, depending upon airspeed and body angle. Plan area of the body was chosen as the reference area for the calculation of force coefficients because of the conventional practice of using wing planform area to calculate force coefficients for wings. This is a somewhat arbitrary decision but is consistent with an interest in the lift forces produced by the body. By using the area data presented in Table 1, however, it is possible to calculate drag coefficients based on frontal area, which can then be compared with other published results. At an *Re* of 1000, the mean drag coefficient for bumblebee worker bodies, based on frontal area at a body angle of 0°, was 1·0, decreasing to 0·63 at an *Re* of 4000; all *Re* values are based on body length. These drag coefficients may be compared with those for a locust (Weis-Fogh, 1956) and a cockchafer beetle (Nachtigall, 1964); coefficients based on frontal area, with the body arranged approximately parallel to the air stream, were approximately 1·47 and 0·48 at *Re* values of 8000 and 4000, respectively (Vogel, 1981). Hocking (1953) determined drag coefficients, based on frontal area at a body angle of approximately 0°, of 1·1 for larger flies (Tabanidae, Culicidae), and values of up to 2·3 for smaller species. A *Drosophila* body at the much lower *Re* of 300 has a drag coefficient based on frontal area equal to 1·16 (Vogel, 1981), while for pigeons and vultures the body

drag coefficient based on frontal area was found by Pennycuick (1968*a*, 1971) to be approximately 0·43 over an *Re* range from 10^3 to 10^6.

The drag coefficient values for bumblebee queens and workers (Fig. 3A,B and the results quoted above) may be compared with those of simple geometrical objects at similar *Re* values. A sphere has a C_D of 1·0 at $Re \approx 10^2$, decreasing to 0·4 at $Re \approx 3 \times 10^3$ and remaining at 0·4 for $Re \approx 10^4$. The infinite cylinder, with flow normal to its long axis, has a C_D of 1·1 at $Re \approx 10^3$, decreasing to 1·0 at $Re \approx 10^4$ (Hoerner, 1958). No source could be found for drag coefficients of streamlined bodies in this *Re* range. However, Hoerner (1958) presents equations which yield approximate values based upon considerations of the pressure drag of spheroids and the additional skin friction drag of a streamlined body. A streamlined body with a maximum ratio of thickness to length of 37 % is predicted to have a C_D based on plan area of 0·24 at an *Re* of 10^3, decreasing to 0·18 at an *Re* of 10^4. A body with maximum ratio of thickness to length of 25 % is predicted at an *Re* of 10^3 to have a C_D based on plan area of 0·16, decreasing to 0·1 at an *Re* of 10^4. The lower ratio of thickness to length is most appropriate for comparison with bumblebees, given their mean body diameter (Dudley & Ellington, 1989). The body drag coefficients obtained in the present study are similar to those for the sphere and are generally greater than those of the aforementioned streamlined bodies; the values thus fall between the extremes of fully separated and streamlined flow.

Some indication of the significance of streamlining may be given by considering the ratio of drag forces on the body facing into the wind to the forces acting on the body when reversed by 180°. Over the airspeed range of 3–5 $m\,s^{-1}$, this ratio averaged 1·53 for a bumblebee queen and 1·45 for a bumblebee worker; these values are not significantly different. The ratios for bumblebees may, however, be compared with the results for *Drosophila* at the much lower *Re* of 300 (Vogel, 1981); drag on a reversed fuselage increased by only 10 %, at airspeeds between 1 and 2 $m\,s^{-1}$. Effects of streamlining are more pronounced at higher *Re*, which probably accounts for the greater reversed drags of bumblebees in comparison with *Drosophila*. Drag forces on the reversed bumblebee fuselages may be particularly high because of the generally posteriorly pointing hairs on the abdomen. As has been noted by Vogel (1981), however, the ratio of body drag to weight is generally small for flying insects, and drag minimization in these cases may not be particularly important.

The decrease of body drag coefficients with increasing *Re* (Fig. 3A,B) is of interest in that parasite drag and concomitant parasite power may not increase as rapidly at higher flight speeds as had been previously considered, or alternatively may be higher at lower speeds. Drag coefficients of streamlined bodies, aerofoils and strut sections generally decrease as *Re* increases from 10^3 to 10^5, while the coefficients of spheres and circular cylinders are approximately constant in the *Re* range 10^3–10^5 and increase at lower *Re* values (Hoerner, 1958). Results similar to those of the current study can be seen in the drag data for insect bodies given by Hocking (1953), Weis-Fogh (1956), Vogel (1966) and Chance (1975); in none of

these studies does drag increase directly in proportion with the square of the airspeed. Lift coefficients also show, in common with drag coefficients, a tendency to decrease with increased *Re* over the range tested (Fig. 4A,B).

A decrease in the drag coefficient with decreased body angle was also observed (Fig. 3A,B) and, since body angle decreases with increased flight speed in bumblebees (Dudley & Ellington, 1990), parasite drag and power are even further reduced. Rayner (1979) discusses for avian flight the possible effects of body tilt on the body drag coefficient, and models these effects by the form of the equation for the drag of a tilted circular cylinder. Csicsáky (1977) presents drag data for models of zebra finch bodies which show a dependence of the drag coefficient upon the body angle similar in form to that of Rayner's model, although the coefficients are of a lower absolute magnitude. The construction of power curves relating mechanical power output to forward velocity of flying animals (e.g. Pennycuick, 1975) will in future need to incorporate the effects of changes in body drag coefficients resulting from varying body angles and *Re* over the range of flight speeds being considered. The power curves presented above for bumblebees in forward flight include the effects of variable body drag coefficients. Until a more precise characterization of the flow field around the body is available, it is probably best not to introduce the induced velocity into such force calculations.

Body lift

Lift forces on insect bodies have been found, with one exception, to be generally less than 10 % of the body weight for airspeeds and angles of attack representative of forward flight. Hocking (1953) claimed that, for a honeybee at maximum flight speed, up to one-third of the body weight could be supported by lift on the fuselage; however, measurements with the current experimental setup of body lift on a 157 mg honeybee revealed that only 8 % of the insect's weight was supported by body lift at a body angle of 15° and an airspeed of $5\,m\,s^{-1}$, increasing to 14 % at a body angle of 45°. Nachtigall (1964) showed that for a cockchafer beetle only 3 % of the body weight was supported by the body lift, at an airspeed of $2{\cdot}25\,m\,s^{-1}$ and a fairly high body angle of 40°. Wood (1970) found that only very small amounts of lift were produced by dipteran bodies, typically 4 % of the body weight at velocities of $2\,m\,s^{-1}$ and a body angle of 10°. Chance (1975) measured body lift forces equal to 10 % of the body weight for a noctuid moth, at an airspeed of $4\,m\,s^{-1}$ and a body angle of 26°. Csicsáky (1977) has measured lift forces equal to 15 % of the body weight on models of zebra finch bodies, at an airspeed of $4{\cdot}5\,m\,s^{-1}$ and a body angle of 25°. Using the morphological data of Table 1 and the measured lift coefficients to calculate lift forces, it can be shown that, for bumblebees, body lift at the body angles typical of forward flight is less than 10 % of the total weight of the animal, a small but nonetheless significant amount that should be taken into account in any analysis of the overall force balance.

Wing characteristics

Measurements of drag forces on real insect wings reflect the contribution of both

profile drag and induced drag, the latter being a consequence of the tip vortices formed on a wing of finite span. Profile drag is composed of pressure drag and skin friction, the former resulting from the separation of flow from the wing prior to reaching the trailing edge, and the latter a consequence of viscous forces in the boundary layer. For wings of elliptical planform, the induced drag coefficient $C_{D,ind}$ is typically estimated from the following formula:

$$C_{D,ind} = C_L^2/\pi \mathcal{A}R , \tag{19}$$

where $\mathcal{A}R$ is the aspect ratio of the wing pair. The planform of bumblebee wings is not elliptical and, moreover, for these wings the relationship between the total drag coefficient and the square of the lift coefficient is not linear, as has similarly been reported for a variety of bird wings (Withers, 1981); induced drag coefficients, and hence profile drag coefficients, cannot therefore be estimated using equation 19. As noted by Ellington (1984*b*), the induced drag coefficient is minimal when lift on the wing is zero, and to estimate the minimum profile drag coefficient it is sufficient to consider the minimum drag coefficient measured for a wing. These values typically range from 0·3 to 0·1 for bumblebee wings at *Re* between 200 and 1200.

It is useful to compare the minimum drag coefficients measured for bumblebee wings with theoretical predictions. The theoretical value of the drag coefficient $C_{D,f}$ of a flat plate oriented parallel to flow, with drag forces being solely attributable to skin friction, is given by (Prandtl & Tietjens, 1957):

$$C_{D,f} = 1{\cdot}33Re^{-1/2} . \tag{20}$$

Values of $C_{D,min}$ for real bumblebee wings reflect a small additional component of pressure drag, and are 2–3 times the theoretical values for flat plates (Table 2); a similar result was found for *Drosophila* wings (Vogel, 1967). The variation of $C_{D,min}$ with *Re* for the bumblebee worker of Fig. 8 is very similar to that derived from the data on *Drosophila* wings (Ellington, 1984*b*). For the bumblebee wing, $C_{D,min} = 4{\cdot}84Re^{-0{\cdot}52}$, while for *Drosophila*, $C_{D,min} = 4{\cdot}8Re^{-0{\cdot}50}$.

Lift on insect wings initially increases with increasing angle of attack to some maximum value. The lift coefficient C_L for a theoretical aerofoil of infinite span under steady-state conditions can be derived as $C_L = 2\pi\alpha'$, where α' is the angle (in radians) of incidence of the aerofoil measured with respect to the zero-lift angle. The slope of the lift–incidence curve at small angles of incidence is therefore 2π, and this value decreases with the aspect ratio for wings of finite span. In the range of α' from 0° to 5°, $dC_L/d\alpha'$ ranges from 2·0 to 0·9 for bumblebee wings, values which are generally lower than previously published results for insect wings (Ellington, 1984*b*). For example, $dC_L/d\alpha'$ is 2·2 for a flat *Drosophila* wing and 4·0 for a *Tipula* wing.

The three-dimensional, corrugated character of insect wings may result in bubbles of air being trapped between the veins of the wings, increasing the effective profile of the wing (Newman *et al.* 1977). Leading-edge separation bubbles may have a similar effect (Ellington, 1984*b*). If the effective profile of the

wing changes with angle of attack, net air circulation about the wing could also change and result in lift coefficients different from those of the theoretical calculation. The slope of the lift–incidence curve is very dependent upon the circulation distribution, as is clear from considering the effects of wing camber. Cambering of model *Drosophila* wings increased the slope of the lift–incidence curve by about 20 % (Vogel, 1967).

Conventional aerofoils in the *Re* range 10^2–10^3 have a maximum C_L of about 0·85 (Hacklinger, 1964), while theoretical calculations of maximum lift coefficients at low *Re* suggest values of less than 1 (Liebeck & Ormsbee, 1970). For the locust forewing, $C_{L,max}$ is about 1·13 at an *Re* of 4000 (Jensen, 1956), about 0·90 at an *Re* of 1200 for a damselfly wing (Rudolph, 1976), about 0·85 for a *Tipula* wing at an *Re* of 1000 (Nachtigall, 1977) and 0·87 for a *Drosophila* wing at an *Re* of 200 (Vogel, 1967). These values of $C_{L,max}$ are somewhat higher than the values for *Bombus terrestris* wings, which range from 0·8 to 0·6 at *Re* between approximately 500 and 1500. As has been previously reported for insect wings, the abrupt stall after the attainment of maximum lift, which is typical of aerofoils at higher *Re*, does not occur. Instead, the lift coefficient declines after this point only gradually from its maximum value. Leading-edge separation bubbles apparently increase the effective camber of the wing and inhibit stalling by causing the reattachment of the separated boundary layer (Ellington, 1984*b*).

The decrease of $C_{L,max}$ with increased *Re* (see Table 2) is an unexpected phenomenon of considerable interest. Nachtigall (1981), in a study on models of locust wings, showed that as the Reynolds number increased from $1{\cdot}1\times10^4$ (mistakenly given in the original paper as $1{\cdot}1\times10^3$) to $2{\cdot}0\times10^4$, the maximum lift coefficient of a flat wing model decreased from 0·85 to 0·80, and that of a wing modelling the downstroke profile decreased from 1·25 to 1·15. Surprisingly, $C_{L,max}$ of a wing modelling the upstroke profile increased from 1·05 to 1·15 over the same Reynolds number range. Ellington (1984*b*) has emphasized the significance of leading-edge bubbles in changing the effective profile, and hence aerodynamic characteristics, of aerofoils with thin leading edges in this *Re* range; it seems likely that the observed variation in $C_{L,max}$ is a consequence of spatial and temporal changes in the leading-edge bubble formed on bumblebee wings. For example, an increase in the frequency of vortex shedding from the wing, as would occur at higher *Re*, might result in smaller leading-edge bubbles with lower circulations, reducing the mean lift of the wing.

Trailing-edge wing flaps are used primarily to increase the lift of a wing (with a concomitant drag increase) at low airspeeds. Hoerner & Borst (1975) review experimental results for a wide variety of trailing-edge flaps. The wing profiles visible in high-speed films (Dudley & Ellington, 1990) at the end of half-strokes seem most similar to the ordinary or plain type of flap, in which the posterior region of the wing is set at some angle relative to the anterior region. Significant flow separation above the plain flap means that lift coefficients are not as high as they might be otherwise (in cases of slotted or split wing flaps), and that drag forces on the wing are significantly increased. For a flapped rectangular model

wing at an Re of 6×10^5, lift coefficients increase with increased angle of attack from $\alpha=-15°$ to $\alpha=+13°$ or so, and then drop sharply (Hoerner & Borst, 1975). Increasing flap deflection at a low angle of attack results in higher lift coefficients up to flap deflections of approximately 70°, after which lift coefficients slowly decline. The results for bumblebee wings and wing models show that lift coefficients are increased by a flap-deflected high wing at higher angles of attack than is the case at higher Re. (Drag forces are also increased, as indicated by the decrease in lift-to-drag ratios for flapped bumblebee wings; see Table 2.) Jensen (1956) showed that the flap profile typical of the late downstroke in the locust increased maximum lift coefficients of the wing. Nachtigall (1981), investigating similar wing configurations, showed that flapped wing profiles during the downstroke generated higher lift forces at small and medium angles of attack than did a flat wing, but produced less lift at high angles of attack. Although flapped wing profiles in the forward flight of bumblebees are most pronounced at the end of half-strokes, when translational velocities are lowest, some increase in lift forces seems likely.

Force coefficients

The mean coefficient method is a useful technique for estimating the lift and power requirements of flying animals. In bumblebees, effective angles of incidence of the wings were demonstrated to be constant from the downstroke to the upstroke, thereby satisfying the assumptions of the mean coefficient method. Although it is tempting to solve for unique values of the mean lift and drag coefficients using the vertical and horizontal force balances, it is probably best not to use the horizontal force balance for this purpose. Calculated horizontal components of the wing lift and drag are very dependent upon estimates of the relative velocity and effective angle of incidence, which for flapping wings are difficult to specify precisely. The approximation of the induced velocity field by a constant induced velocity along the wing and through the wingbeat will introduce an unknown inaccuracy into such estimates. It is, however, sufficient to consider a range of likely mean drag coefficients to determine lift and power requirements of forward flight. Fortunately, mean lift coefficients calculated considering only the vertical force balance are almost independent of the assumed mean drag coefficient over the likely range of values.

Mean lift coefficients for bumblebees in forward flight, calculated according to quasi-steady aerodynamic theory, were never less than one, while maximum lift coefficients measured on bumblebee wings under conditions of steady-state flow generally did not exceed one. Cambering and flap-deflected hindwings were demonstrated to improve the lifting performance of wings, but not to the extent required for maximum lift coefficients to exceed the calculated mean lift coefficients. Ellington (1984*d*) demonstrated that, in hovering flight, unsteady aerodynamic mechanisms are required to generate the requisite forces for weight support. This finding, in conjunction with the present results, indicates that for

flying bumblebees unsteady aerodynamic mechanisms are operating at *all* airspeeds examined, from hovering to fast forward flight.

Furthermore, lift forces on the wings will be less than those predicted by the quasi-steady analysis because of the Wagner effect (Ellington, 1984*b*), the time-dependent growth of the circulation and lift to steady-state values. For example, after six chords of travel, lift on a wing section starting from rest is only 90 % of the quasi-steady value. In hovering flight, when the distance travelled by a wing chord is least, the Wagner effect should be more prominent than in forward flight. Even at a flight speed of $4{\cdot}5\,m\,s^{-1}$, bumblebee wings travel only about seven chord lengths during the downstroke and a much smaller distance during the upstroke, so the Wagner effect is still important. It may therefore be concluded even more strongly that unsteady effects are acting in the forward flight of bumblebees.

In addition to the quasi-steady analysis, unsteady wing theories have also been applied to flapping animal flight (e.g. Möllenstädt, 1980; Phlips *et al.* 1981). In these theories, the temporal variations in wing motion are assumed to be small, and the wake does not move under its own velocity field. These approximations are not realistic for the hovering flight of insects (Ellington, 1984*c*) and, given the advance ratios typical for bumblebees in forward flight, are also not appropriate for the present study. Vortex theories have also been developed for forward animal flight (Cone, 1968; Rayner, 1979). These theories offer refined estimates of the induced velocity and induced power requirement given a particular aerodynamic mechanism, but do not evaluate the likelihood of this mechanism actually operating in flight. Even simplified versions of the vortex theory involve excessive computation and, because of assumptions concerning the wake geometry, are not appropriate for the low advance ratios typically found for flying insects.

Possible aerodynamic mechanisms for improving the lift performance of insect wings have been discussed by Ellington (1984*b*). Delayed stall, whereby transient high lift is produced on an aerofoil at angles of attack greater than the stalling angle, could increase lift. A translating aerofoil with a simultaneously increasing angle of attack also experiences increase lift (Kramer's effect). In hovering flight, effective angles of incidence rule out both these mechanisms as candidates for producing the lift required for weight support, and a similar argument suggests that these mechanisms of lift enhancement are also not particularly significant in forward flight. Wing rotation *per se* at either end of the wingbeat is, however, likely to be of greater significance. Circulation is produced by both wing translation and wing rotation; calculations for hovering flight show that the circulation associated with rotation at the ends of half-strokes is comparable to the circulation associated with translation (Ellington, 1984*b*). Although rotation decreases, and translation during the downstroke increases, with increased airspeed, translation during the upstroke is nonetheless approximately equal to or even less than that in hovering flight, and the circulation resulting from wing rotation may therefore still be comparable to that of wing translation. Ellington (1984*b*) proposed for hovering flight a mechanism based upon the observed wing flexion during rotation which would allow the circulation associated with wing

rotation to be used advantageously on the following half-stroke. Wing flexion similar to that described for hovering flight was a feature of forward flight in bumblebees (Dudley & Ellington, 1990), although the extent of flexion was progressively reduced at higher airspeeds. This may be correlated with the reduction in the mean lift coefficient at higher airspeeds.

The analysis of pitching moments indicated that pitching moments predicted by a quasi-steady analysis were, in general, well in excess of those required to produce the body angles observed in free flight. This result suggests that lift production is not symmetrical about the mean positional angle $\bar{\phi}$, as is predicted by the quasi-steady analysis for a wing in simple harmonic motion. By varying lift production at the ends of half-strokes, possibly by different angular velocities of wing rotation or by controlling wing separation, the lift distribution over the wingbeat could be controlled so as to produce the pitching moments necessary for forward flight.

The relative contributions to vertical force production of the downstroke and upstroke were demonstrated to change gradually with airspeed: the downstroke progressively became more important in the production of vertical force as airspeed increased. Little, or even negative, vertical force was produced by the upstroke at the higher airspeeds examined. Since in the downstroke the wings are moved forwards and downwards, and are moved downwards at a steeper stroke plane angle as airspeed increases, it is not surprising that the downstroke gradually assumes a greater importance in weight support with increased airspeed.

A quantitative treatment of the relative contributions to thrust generation of the downstroke and upstroke was not possible, because of the aforementioned problems with the horizontal force balance. It is probable, however, that the upstroke is primarily associated with thrust production and contributes little to weight support. It is clear that the wing is aerodynamically active during the upstroke, because effective angles of incidence during the upstroke were positive and of approximately the same magnitude as those during the downstroke. The positive effective angles of incidence indicate that, during forward flight, lift on the wing will be directed forwards and upwards, while wing drag will be directed forwards and downwards. Vertical components of the wing lift and drag are therefore of opposite sign, and the net effect of the upstroke will be primarily the production of a horizontal force. This interpretation is in accord with the finding that vertical forces produced during the upstroke are small compared to those produced during the downstroke. The magnitude of the horizontal force produced during the upstroke will tend to increase with increased airspeed, because the lift on the wing during the upstroke will point progressively more forward. This gradual change in the direction of wing lift during the upstroke occurs because of the constancy in effective angles of incidence coupled with the increase in stroke plane angle that accompanies an increase in forward airspeed. Fig. 16 summarizes for different airspeeds the wing orientations and directions of forces produced during the downstroke and upstroke.

There is unfortunately little information available on the aerodynamic role of

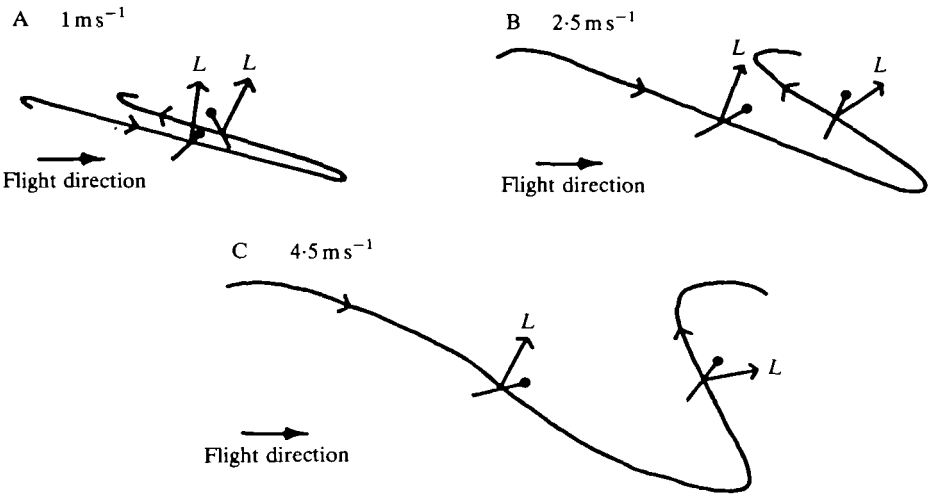

Fig. 16. Wing tip paths, wing orientation and direction of lift forces (L) during the downstroke and upstroke for the bumblebee BB01 in free flight at various flight speeds. The arrows indicate the direction of flight. Wing motion is sinusoidal. Effective angles of incidence were calculated using mean kinematic parameters for the airspeed range, and incorporate effects of the induced velocity. The wing section represented is the most proximal one-third of the wing (Dudley & Ellington, 1990); qualitatively the arguments are equivalent for other wing sections. Magnitudes of the lift are not scaled according to relative velocity of the wing section.

the upstroke in the forward flight of insects. Jensen (1956) concluded for a tethered desert locust that the downstroke was primarily responsible for lift and thrust production, with the upstroke contributing only a small amount of thrust to the net force balance. Jensen's analysis, as mentioned previously, relied upon only approximate calculations of effective angles of incidence, and also probably used erroneous force coefficients for the wings (Ellington, 1984*b*); it should therefore be treated with some caution. Brodskii & Ivanov (1984), using flow visualization, showed for a tethered skipper (*Adopaea lineola* Ochs.) that the upstroke is aerodynamically active and contributes primarily to the production of thrust. This experimental result is in accord with the above discussion on the role of the upstroke, although it should be emphasized that skippers have a wing loading and wingbeat frequency much lower than those of bumblebees.

In contrast to the situation for insects, there now exist considerable data about the aerodynamic role of the upstroke in the forward flight of bats and birds. Rayner *et al.* (1986) demonstrated, using flow visualization, that in the noctule bat the function of the upstroke changes as forward airspeed changes. Aerodynamic lift on the wing, resulting primarily in thrust, was generated during the upstroke at high airspeeds. No significant lift was produced by the wing during the upstroke at low flight speeds. In the long-eared bat, for which Norberg (1976) had deduced a weak lift on the wing during the upstroke, producing primarily thrust, Rayner *et al.* (1986) could find no evidence that the upstroke is active at any speed, although

very weak lift may not be visible by flow visualization. Aldridge (1986) investigated the effective angles of incidence and the wing path characterizing the forward flight of the greater horseshoe bat. He concluded that at low flight speeds thrust was generated during the upstroke, while at high speeds the upstroke contributed to weight support and generated a negative thrust. It has been shown experimentally for the slow flight of the pigeon (Spedding *et al.* 1984) and of finches (Kokshaysky, 1979) that the upstroke does not contribute significantly to the force balance. Diverse aerodynamic functions of the upstroke in the forward flight of bats and birds have thus been demonstrated. A reconstruction using flow visualization of the vortex wake of insects in free flight would permit an experimental evaluation of the roles deduced above for the aerodynamic function of the downstroke and upstroke in the forward flight of bumblebees.

The widespread belief that bumblebee flight is incompatible with quasi-steady aerodynamics is well supported here. As best we can determine, the first quantitative demonstration that mean lift coefficients characterizing bumblebee flight are in excess of quasi-steady values was that of Osborne (1951). In contrast, it has generally been assumed by biologists that quasi-steady aerodynamics are sufficient to produce the forces required in the fast forward flight of insects. This is based primarily on the results of Jensen (1956) for tethered locusts. It is, however, unlikely that quasi-steady aerodynamics characterize even fast forward flight in locusts: Cloupeau *et al.* (1979) have shown that at high advance ratios the vertical forces produced by tethered locusts are well in excess of those predicted by quasi-steady theory. Using free-flying bumblebees as a case study, we have shown that fast forward flight is incompatible with quasi-steady aerodynamics. The exact nature of the unsteady aerodynamic mechanisms characterizing insect flight is clearly of importance in understanding the evolutionary success of the Insecta and, as such, merits extensive investigation.

Mechanical power output

No consistent trend relating mechanical power output and forward airspeed was observed for bumblebees in free flight, although in some cases very shallow U-shaped curves were evident. Parasite power at the airspeeds considered was always small in magnitude. Therefore, at these airspeeds, calculations of body drag using variable body drag coefficients will not produce power calculations substantially different from those assuming a constant value. In contrast to parasite power, profile power was always a significant component of total power requirements, and increased markedly from 1 to 4·5 m s^{-1}. This increase in profile power, coupled with a comparable decrease in induced power, resulted in an approximately constant aerodynamic power requirement over the range of airspeeds considered, largely accounting for the flatness of the mechanical power curve. It is noteworthy that straightforward application of a Pennycuick-type model with the assumption of a constant profile power component would predict very pronounced U-shaped power curves with deep minima. The general correspondence between the present calculations of mechanical power output at

low speeds, and those calculated by Ellington (1984*d*) using a more detailed aerodynamic model, suggests that the values of mechanical power requirements determined in the present study are reliable.

If flight muscle efficiency does not vary with forward airspeed, then metabolic power input will parallel mechanical power output and similarly remain approximately constant from hovering to fast forward flight. Changes in muscle efficiency will most probably be correlated with changes in contraction mechanics of the muscle. As demonstrated above, the magnitude of the resultant force vector produced in forward flight by the beating wings is relatively constant over the range of airspeeds examined. Only the direction of the vector changes, pointing slightly more forward as airspeed increases. Since muscle strain and strain rate are also unlikely to change with airspeed, given the generally invariant wing kinematics, large changes in muscle efficiency over the range of airspeeds considered would be surprising.

The maximum power output of fibrillar flight muscle is not likely to exceed $200\,W\,kg^{-1}$ of muscle (Ellington, 1984*d*; Ellington, 1985). Given the total mass of flight muscle of a flying animal, it is therefore possible to determine its maximum power output. Thoracic masses for those insects filmed in free flight were given, as a fraction of body mass, in Dudley & Ellington (1990). J. H. Mayberry (personal communication) has determined for *Bombus pascuorum* queens, workers and drones a mean ratio of flight muscle mass to thoracic mass of 0·87 ($N = 12$, S.D. = 0·03). Using this ratio for *Bombus terrestris*, the ratio of flight muscle mass to body mass is about 30%, and the mean maximum power output of the bumblebees filmed in free flight is then approximately $56\,W\,kg^{-1}$ body mass. Comparing this result to the values of mechanical power output given zero elastic energy storage (Fig. 15), it can be seen for most of the bumblebee sequences examined that the maximum power available from the flight muscle exceeds the mechanical power required when there is no elastic storage of energy. Thus, on the grounds of power requirements alone, elastic energy storage cannot be deemed essential in forward flight, as some power supplementary to aerodynamic requirements is available to oscillate the wings. Ellington (1984*d*) concluded for bumblebees that little energy was available for inertial power requirements. However, his calculations were based on a ratio of flight muscle mass to body mass of 0·14, as given by Greenewalt (1962), which is about half the actual value for bumblebees.

Comparing mechanical power outputs with and without elastic energy storage, it is clear that substantial energy savings can result if the kinetic energy of the oscillating wing mass and wing virtual mass is stored elastically at the end of a half-stroke and used to accelerate the wing in the following half-stroke. As identified principally by Weis-Fogh (1959, 1965, 1972, 1973), likely elastic components of the flight system are the skeletal cuticle, protein elastomers (e.g. resilin) and the flight muscle itself. The relative importance of these components is not known, although Ellington (1984*d*) concluded that the fibrillar flight muscle of Hymenoptera must act as a substantial energy store (see also Alexander & Bennet-Clark, 1977).

Indeed, the flight muscle alone may be capable of storing all the kinetic energy involved in a half-stroke. Given that the maximum energy that can be stored elastically in fibrillar muscle is about $1{\cdot}3\,J\,kg^{-1}$ muscle (Alexander & Bennet-Clark, 1977), the total energy that can be stored in the muscles of the bumblebees filmed in free flight may be calculated. For the three bumblebees, the kinetic energy of a half-stroke was only about half the maximum that could be stored by the muscle mass (about $0{\cdot}76\,J\,kg^{-1}$ muscle). Thus, the flight muscles alone could store all the kinetic energy of the oscillating wings. This conclusion is opposite to that of Ellington (1984*d*), who calculated lower values for the maximum kinetic energy that could be stored in the flight muscle. In the present study, the larger ratios of flight muscle mass to body mass, as mentioned above, account for the greater values of energy storage in the flight muscle.

We are grateful to the late Dr Ken Machin for his invaluable advice and discussion during the course of this study. Mr Steve Ellis kindly built the transducer used to measure aerodynamic forces. We thank Dr Ulla Norberg and two anonymous reviewers for comments. The Marshall Commission, the Smithsonian Tropical Research Institute, and the Science and Engineering Research Council provided financial support.

References

ALDRIDGE, H. D. J. N. (1986). Kinematics and aerodynamics of the greater horseshoe bat, *Rhinolophus ferrumequinum*, in horizontal flight at various flight speeds. *J. exp. Biol.* **126**, 479–497.

ALEXANDER, R. McN. & BENNET-CLARK, H. C. (1977). Storage of elastic strain energy in muscle and other tissues. *Nature, Lond.* **265**, 114–117.

ALFORD, D. V. (1975). *Bumblebees*. London: Davis Poynter.

BERGER, M. (1985). Sauerstoffsverbrauch von Kolibris (*Colibri coruscans* and *C. thalissinus*) beim Horizontalflug. In *BIONA Report* **3** (ed. W. Nachtigall), pp. 307–314. Akad. Wiss., Mainz: G. Fischer.

BERNSTEIN, M. H., THOMAS, S. P. & SCHMIDT-NIELSEN, K. (1973). Power input during forward flight in the Fish Crow *Corvus ossifragus*. *J. exp. Biol.* **58**, 401–410.

BRAMWELL, A. R. S. (1976). *Helicopter Dynamics*. London: Edward Arnold.

BRODSKII, A. K. & IVANOV, V. D. (1984). Rol' virkhyei v polyetye nasyekomyikh. (The role of vortices in insect flight.) *Zool. Zh.* **63**, 197–208.

CARPENTER, R. E. (1985). Flight physiology of flying foxes, *Pteropus poliocephalus*. *J. exp. Biol.* **114**, 619–647.

CHANCE, M. A. C. (1975). Air flow of the flight of a noctuid moth. In *Swimming and Flying in Nature*, vol. 2 (ed. T. Y. Wu, C. J. Brokaw & C. Brennen), pp. 829–843. New York: Plenum Press.

CLOUPEAU, M., DEVILLIERS, J. F. & DEVEZEAUX, D. (1979). Direct measurements of instantaneous lift in the desert locust; comparison with Jensen's experiments on detached wings. *J. exp. Biol.* **80**, 1–15.

CONE, C. D. (1968). The aerodynamics of flapping bird flight. *Spec. Scient. Rep. Va. Inst. Mar. Sci.* No. 52.

CSICSÁKY, M. J. (1977). Body gliding in the zebra finch. *Fortschr. Zool.* **24**, 275–286.

DUDLEY, R. & ELLINGTON, C. P. (1990). Mechanics of forward flight in bumblebees. I. Kinematics and morphology. *J. exp. Biol.* **148**, 19–52.

ELLINGTON, C. P. (1984*a*). The aerodynamics of hovering insect flight. I. The quasi-steady analysis. *Phil. Trans. R. Soc. Ser.* B **305**, 1–15.

ELLINGTON, C. P. (1984*b*). The aerodynamics of hovering insect flight. IV. Aerodynamic mechanisms. *Phil. Trans. R. Soc. Ser.* B **305**, 79–113.

ELLINGTON, C. P. (1984*c*). The aerodynamics of hovering insect flight. V. A vortex theory. *Phil. Trans. R. Soc. Ser.* B **305**, 115–144.

ELLINGTON, C. P. (1984*d*). The aerodynamics of hovering insect flight. VI. Lift and power requirements. *Phil. Trans. R. Soc. Ser.* B **305**, 145–181.

ELLINGTON, C. P. (1985). Power and efficiency of insect flight muscle. *J. exp. Biol.* **115**, 293–304.

GREENEWALT, C. H. (1962). Dimensional relationships for flying animals. *Smithsonian Misc. Collns* **144**, 1–46.

GREENEWALT, C. H. (1975). The flight of birds. *Trans. Am. Phil. Soc.* **65**, part 2.

HACKLINGER, M. (1964). Theoretical and experimental investigation of indoor flying models. *J. R. aero. Soc.* **68**, 728–734.

HOCKING, B. (1953). The intrinsic range and speed of flight of insects. *Trans. R. ent. Soc. Lond.* **104**, 223–345.

HOERNER, S. F. (1958). *Fluid-dynamic Drag*. Brick Town, NJ: S. F. Hoerner.

HOERNER, S. F. & BORST, H. V. (1975). *Fluid-dynamic Lift*. Brick Town, NJ: Hoerner Fluid Dynamics.

JENSEN, M. (1956). Biology and physics of locust flight. III. The aerodynamics of locust flight. *Phil. Trans. R. Soc. Ser.* B **239**, 511–552.

KAMMER, A. E. & HEINRICH, B. (1978). Insect flight metabolism. In *Advances in Insect Physiology*, vol. 13 (ed. J. E. Treherne, M. J. Berridge & V. B. Wigglesworth), pp. 133–228. London: Academic Press.

KOKSHAYSKY, N. V. (1979). Tracing the wake of a flying bird. *Nature, Lond.* **279**, 146–148.

LIEBECK, R. H. & ORMSBEE, A. I. (1970). Optimization of airfoils for maximum lift. *J. Aircraft.* **7**, 409–415.

MARGARIA, R. (1968). Positive and negative work performance in human locomotion. *Int. Z. angew. Physiol. einschl. Arbeitsphysiol.* **25**, 339–351.

MÖLLENSTÄDT, W. (1980). Einige Grundzüge der instationären Aerodynamik harmonisch schwingender Tierflügel in inkompressibler, reibungsfreier Strömung. In *Instationäre Effekte an Schwingenden Tierflügeln* (ed. W. Nachtigall), pp. 9–34. Wiesbaden: Franz Steiner.

NACHTIGALL, W. (1964). Zur Aerodynamik des Coleopterenfluges: wirken die Elytren als Tragflügel? *Verh. Dt. Zool. Ges. (Kiel).* **58**, 319–326.

NACHTIGALL, W. (1977). Die aerodynamische Polare des Tipulaflügels und eine Einrichtung zur halbautomatischen Polarenaufnahme. In *The Physiology of Movement; Biomechanics* (ed. W. Nachtigall), pp. 347–352. Stuttgart: Fischer.

NACHTIGALL, W. (1981). Der Vorderflügel grosser Heuschrecken als Luftkrafterzeuger. I. Modelmessungen zur aerodynamischen Wirkung unterschiedlicher Flügelprofile. *J. comp. Physiol.* **142**, 127–134.

NEWMAN, B. G., SAVAGE, S. B. & SCHOUELLA, D. (1977). Model tests on a wing section of an *Aeschna* dragonfly. In *Scale Effects in Animal Locomotion* (ed. T. J. Pedley), pp. 445–477. London: Academic Press.

NORBERG, U. M. (1976). Aerodynamics, kinematics, and energetics of horizontal flapping flight in the long-eared bat *Plecotus auritus*. *J. exp. Biol.* **65**, 459–470.

OSBORNE, M. F. M. (1951). Aerodynamics of flapping flight with application to insects. *J. exp. Biol.* **28**, 221–245.

PENNYCUICK, C. J. (1968*a*). A wind-tunnel study of gliding flight in the pigeon *Columba livia*. *J. exp. Biol.* **49**, 509–526.

PENNYCUICK, C. J. (1968*b*). Power requirements for horizontal flight in the pigeon *Columba livia*. *J. exp. Biol.* **49**, 527–555.

PENNYCUICK, C. J. (1971). Control of gliding angle in Ruppell's griffon vulture *Gyps ruppelli*. *J. exp. Biol.* **55**, 39–46.

PENNYCUICK, C. J. (1975). Mechanics of flight. In *Avian Biology*, vol. 5 (ed. D. S. Farner & J. R. King), pp. 1–75. London: Academic Press.

PHLIPS, P. J., EAST, R. A. & PRATT, N. H. (1981). An unsteady lifting line theory of flapping wings with application to the forward flight of birds. *J. Fluid Mech.* **91**, 697–730.

PRANDTL, L. & TIETJENS, O. G. (1957). *Applied Hydro- and Aeromechanics*. New York: Dover.

RAYNER, J. M. V. (1979). A new approach to animal flight mechanics. *J exp. Biol.* **80**, 17–54.

RAYNER, J. M. V., JONES, G. & THOMAS, A. (1986). Vortex flow visualizations reveal change in upstroke function with flight speed in bats. *Nature, Lond.* **321**, 162–164.

REES, C. J. C. (1975*a*). Form and function in insect wings. *Nature, Lond.* **256**, 200–203.

REES, C. J. C. (1975*b*). Aerodynamic properties of an insect wing section and a smooth aerofoil compared. *Nature, Lond.* **258**, 141–142.

RUDOLPH, R. (1976). Die aerodynamischen Eigenschaften von *Calopteryx splendens* (Harris) (Zygoptera: Calopterygidae). *Odonatologica* **5**, 135–140.

SPEDDING, G. R., RAYNER, J. M. V. & PENNYCUICK, C. J. (1984). Momentum and energy in the wake of a pigeon (*Columba livia*) in slow forward flight. *J. exp. Biol.* **111**, 81–102.

THOMAS, S. P. (1975). Metabolism during flight in two species of bats, *Phyllostomus hastatus* and *Pteropus gouldii*. *J. exp. Biol.* **63**, 273–293.

THOMAS, S. P. (1981). Ventilation and oxygen extraction in the bat *Pteropus gouldii* during rest and steady flight. *J. exp. Biol.* **94**, 231–250.

TORRE-BUENO, J. R. & LAROCHELLE, J. (1978). The metabolic cost of flight in unrestrained birds. *J. exp. Biol.* **65**, 471–482.

TUCKER, V. A. (1966). Oxygen consumption of a flying bird. *Science* **154**, 150–151.

TUCKER, V. A. (1972). Metabolism during flight in the laughing gull *Larus atricilla*. *Am. J. Physiol.* **222**, 237–245.

TUCKER, V. A. (1973). Bird metabolism during flight: evaluation of a theory. *J. exp. Biol.* **58**, 589–609.

VOGEL, S. (1966). Flight in *Drosophila*. I. Flight performance of tethered flies. *J. exp. Biol.* **44**, 567–578.

VOGEL, S. (1967). Flight in *Drosophila*. II. Aerodynamic characteristics of fly wings and wing models. *J. exp. Biol.* **46**, 431–443.

VOGEL, S. (1981). *Life in Moving Fluids*. Boston: Willard Grant Press.

WEIS-FOGH, T. (1956). Biology and physics of locust flight. II. Flight performance of the desert locust (*Schistocerca gregaria*). *Phil. Trans. R. Soc. Ser.* B **239**, 459–510.

WEIS-FOGH, T. (1959). Elasticity in arthropod locomotion: a neglected subject, illustrated by the wing system of insects. *XVth int. Congr. Zool.* **4**, 393–395.

WEIS-FOGH, T. (1965). Elasticity and wing movements in insects. *Proc. XIIth int. Congr. Ent.* 186–188.

WEIS-FOGH, T. (1972). Energetics of hovering in hummingbirds and in *Drosophila*. *J. exp. Biol.* **56**, 79–104.

WEIS-FOGH, T. (1973). Quick estimates of flight fitness in hovering animals, including novel mechanisms for lift production. *J. exp. Biol.* **59**, 169–230.

WITHERS, P. C. (1981). An aerodynamic analysis of bird wings as fixed airfoils. *J. exp. Biol.* **80**, 83–91.

WOOD, J. (1970). A study of the instantaneous air velocities in a plane behind the wings of certain Diptera flying in a wind tunnel. *J. exp Biol.* **52**, 17–25.